ES Mater. Manuf., 2021, **12**, 43-52

ES Materials and Manufacturing

DOI: https://dx.doi.org/10.30919/esmm5f1042

Structural, Electronic, and Optical Properties of Lead-Free Halide Double Perovskite Rb_2AgBiI_6: A Combined Experimental and Density Functional Theory Study

Ajinkya Bhorde,[1, 2] Ravindra Waykar,[1, 2] Sachin R. Rondiya,[3] Shruthi Nair,[1, 2] Ganesh Lonkar[4,] Adinath Funde,[1] Nelson Y. Dzade[3,*] and Sandesh Jadkar[1, 2,*]

Abstract

Hybrid lead halide perovskites have emerged as an attractive photoactive semiconductor for optoelectronic applications such as photovoltaics. However, their toxicity and stability issues pose significant challenges to its wide-scale applications and hence the need to find alternative perovskites that are stable and environmentally benign. Recently, double perovskites have been suggested as a potential alternative owing to their non-toxicity and high stability. In the present study, we report the first synthesis of Rb_2AgBiI_6 thin films in a cubic crystal structure using a facile room-temperature single-step solution process synthesis method and explore their potential optoelectronic applications. The structural, thermal, and mechanical stability, electronic, and optical properties are studied using various experimental techniques, and the results are further corroborated by first-principles density functional theory (DFT) calculations. The Rb_2AgBiI_6 film has an estimated band gap ~ of 1.98 eV with the demonstrated thermal stability of ~ 440 ºC, suggesting its potential suitability for low-cost thin-film solar cells. The initial fabricated photovoltaic device without optimization of the synthesis conditions and device architecture show power conversion efficiency (PCE) of 0.1 % and an open-circuit voltage (Voc) of 0.46 V. The successful incorporation of Rb in Bi-based double perovskite should open the way to a new class of Rubidium-based perovskites with significant potential for optoelectronic applications.

Keywords: Rb_2AgBiI_6; Lead-free double perovskites; Low-temperature; Solar cell.
Received date: 25 November 2020; Accepted date: 25 January 2021.
Article type: Research article.

1. Introduction

Halide based perovskite solar cells (PSCs) are recently recognized as strong potential candidates for photovoltaic research and development.[1] The organic-inorganic and hybrid organic-inorganic halide perovskite materials are characterized with unique optoelectronic properties such as long term charge carrier diffusion length, high absorption coefficient (10^4-10^5 cm^{-1}), low-cost synthesis,[2] high charge carrier mobility,[3] appropriate band gaps (1.5-2.3 eV),[4] low crystallization energy barrier,[5,6] low trap-state density,[7,8] and low exciton binding energy.[9,10] These germane properties make metal halide perovskites attractive candidates for applications in opto-electronics such as solar cells,[11,12] lasers,[13-14] light-emitting diodes (LED),[14,15] and water splitting.[16,17] ABX_3 organic-inorganic hybrid perovskite materials, particularly $CH_3NH_3PbI_3$, have been widely investigated in recent years, with reported photo conversion efficiency (PCE) exceeding 22 %,[4,18,19] making these materials suitable candidates for replacing commonly employed Si-based solar cells. The hybrid organic-inorganic metal halide perovskite solar cells (PSCs) recorded PCE of 25.2 % and proved it is the most promising technology for next-generation low-cost solar cell.[20] However, the lead toxicity and the intrinsic instability of the bulk lead-halide perovskite materials and their interface hetero-structures have remained a significant drawback to their large-scale applications and commercialization.[21-24] Efforts to replace the Pb in PSCs with low toxic cations, including Sn(II),[25] Ag(I),[26] Bi(III),[27] Ti(IV)[28] and Sb(III)[29] have therefore received

[1] *School of Energy Studies, Savitribai Phule Pune University, Pune 411 007, India*
[2] *Department of Physics, Savitribai Phule Pune University, Pune 411 007, India*
[3] *The School of Chemistry, Cardiff University, Cardiff, CF10 3AT, Wales, UK*
[4] *National Centre for Flexible Electronics, Indian Institute of Technology Kanpur, 208016, India*
* *Email:* sandesh@physics.unipune.ac.in (S.R. Jadkar)

significant attention. Shao *et al.*[30] reported Sn-based $CH_3NH_3SnI_3$ and $FASnI_3$ PSC with the highest PCE, up to 9%.[30] However, organic cations (MA, FA, *etc.*) are characterized by relatively low stability due to facile volatilization. Lead-free inorganic perovskites, including $CsSnI_3$, have demonstrated power conversion efficiency up to 3.31 %.[25] Sn^{2+}-based perovskite devices showed extremely low stability, even under commonly used inert conditions, due to the facile oxidation of Sn^{2+} to Sn^{4+}, making them unfeasible for typical photovoltaic applications. A recent approach towards stable lead-free perovskite materials is the substitution of Pb^{2+} with heterovalent M^{3+} cations. A promising candidate for this type of substitution is non-toxic Bi^{3+}, which is isoelectronic with Pb^{2+}.[31] Bi-based single perovskites such as $CsBi_3I_{10}$,[32] $Cs_3Bi_2I_9$,[33] and double perovskite such as Cs_2AgBiX_6 (X = Br, Cl)[34] have been reported with up to 3.2 % PCE efficiency. Lead-free halide double perovskite Cs2AgBiBr6 was first synthesized by Slavney *et al.*[35], who reported an indirect band gap of ~ 1.95 eV and long-term stability as compare to lead-based perovskites. McClure *et al.*[36] synthesized $Cs_2AgBiBr_6$ and $Cs_2AgBiCl_6$ double perovskites and reported indirect bandgap of 2.19 and 2.77 eV, respectively. Volonakis *et al.*[37] reported stable double perovskite $Cs_2AgBiCl_6$ with a band gap in the range of 1.9-3.0 eV.[37] Despite extensive studies of Cs_2AgBiX_6-based materials (X = Cl, Br, and I), there exists no successful report of the synthesis and characterization of Rubidium-based double perovskite Rb_2AgBiX_6, which makes this investigation timely. Rubidium has atomic radii ~ 265 pm with similar chemical and physical properties as cesium (atomic radii ~ 298 pm). However, synthesis and detailed insights into the structural, mechanical, and optoelectronic properties of Rb-based double perovskite Rb_2AgBiX_6 has not yet been established. Recently, Saliba *et al.* [38] demonstrated that incorporating Rb cations into perovskite solar cells improves their stability and photovoltaic performances. The PEC performance reported for RbCsMAFA perovskite solar cell reached 20.6 %.[38] However, the preparation of high-quality films of Rb-based double perovskite Rb_2AgBiX_6 for optoelectronic applications is challenging, which explains why neither films nor photovoltaic devices based on Rb_2AgBiX_6 double perovskites have not been reported so far. Considering that thin films are critical for making lead-free halide double perovskites accessible for optoelectronic applications, we have developed a solution process single-step synthetic route that allows for the preparation of phase pure, thin films and powders of the double perovskite Rb_2AgBiI_6 at room temperature. We have studied the structural, optical, morphological, and electronic properties of Rb_2AgBiI_6 experimentally and corroborated our results by hybrid DFT calculations. Phase purity and structural properties were investigated using XRD, Raman, and TEM analysis. The optical band gap of the synthesized Rb_2AgBiI_6 films was estimated at ~ 1.98 eV and validated through state-of-the-art hybrid DFT calculations (1.96 eV). Initial attempts to fabricate Rb_2AgBiI_6 based perovskite solar cells and photo detectors using TiO_2 and CuSCN as hole transport material (HTM) and electron transport layer (ETM), respectively, demonstrated PCEs of ~ 0.1 % and a Voc of 0.46 V. There is, however, an enormous opportunity to increase the device efficiency through optimizing material synthesis and device architecture. Additionally, the Rb_2AgBiI_6 films exhibit higher thermal stability of degradation ~ 440 °C under operating conditions as obtained from TGA analysis. These results demonstrated the potential of highly tunable double Rb_2AgBiI_6 perovskite as a novel class of semiconductor materials for optoelectronic applications.

2. Experimental and Theoretical Section

2.1 Synthesis of Rb_2AgBiI_6 Thin film

The ability to synthesize high-quality perovskite materials on a large scale using inexpensive and straightforward methods is essential for commercializing photovoltaic technology. In 2017, Cheng *et al.* synthesized $(CH_3NH_3)_2AgBiI_6$ double perovskite powder through solid-state reaction and investigated its structural and optical properties.[39] Femi *et al.*[40] reported the synthesis of bismuth-based $Cs_2AgBiBr_6$ double perovskite thin films by vacuum-sublimation and solution-processing. A variety of perovskite synthesis methods were reported, including a two-step spin-coating and Vacuum flash-assisted solution process (VASP), vapor deposition, and gas-induced method.[41] All these methods, however, require costly equipment, operations at high temperatures and are time-consuming. In this study, we have employed a one-step solution process (outside the glove box) spin coating method at room temperature (without any solvent treatment) to synthesis double perovskite Rb_2AgBiI_6 films and powders. The one-step solution process and room temperature synthesis method have several merits over the above-mentioned synthesis methods, including easy setup, large-scale deposition, less processing time, and no need for high-temperature synthesis. The setup for one-step solution process spin coating method comprises of 2 M Rubidium Iodide (RbI, 99.9 %: Sigma Aldrich), 1 M Silver Iodide (AgI, 99.9 %: Alfa Aesar), 1 M Bismuth Triiodide (BiI_3, 99.9 %: Sigma Aldrich) added in 1 ml N, N-Dimethylformamide (DMF). The resultant solution was transferred for sonication until it becomes crystal clear. Glass substrates were cleaned via chemical treatment. It was initially washed with soap solution, then with sonicate 15 min in distilled water, and finally transferred into the piranha solution (H_2SO_4:H_2O as 3:2 in volume ratio). After that, the glass was rinsed with distilled water and dried with an air blower. Rb_2AgBiI_6 thin films were deposited on a glass substrate (Corning glass # 7059) by the simple spin coating method (6000 RPM for 30 sec). The prepared Rb_2AgBiI_6 film was annealed at 90 °C on a hot plate for 30 min. The same solution was annealed for 24 hrs on a hot plate to prepare Rb_2AgBiI_6 powder. Fig. 1 depicts the schematic for the facile synthesis process of Rb_2AgBiI_6 double perovskite.

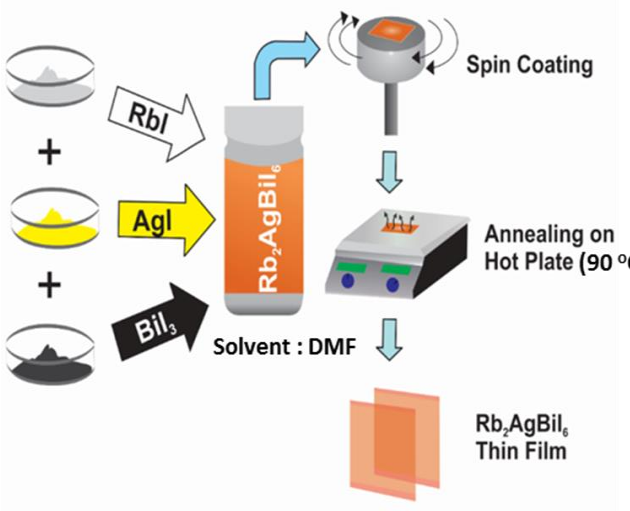

Fig. 1 Schematic representation of the facile synthesis method of Rb_2AgBiI_6 double perovskite, which involved RbI, AgI, and BiI3 as chemical precursors with spin coating and hot plate as a thin film deposition tool.

2.2 Solar cell and Photo-detector Fabrication

Typically, Rb_2AgBiI_6 perovskite solar cells are fabricated on fluorine-doped tin oxide (FTO) coated glass as a substrate. The FTO substrate (anode) was initially clean using soap solution followed by 15 min ultra-sonication in a mixer of distilled water (DW), acetone, and isopropyl alcohol (IPA). One side of the conducting FTO was etched using hydrochloric acid and zinc powder for the device fabrication. A compact TiO_2 layer was deposited on the pre-cleaned FTO substrate using the radio frequency (RF) magnetron sputtering method. The compact TiO_2 (Electron Transport Layer) was deposited at 200-Watt RF power and 1.8×10^{-2} Torr deposition pressure. In the third step, we have deposited the active perovskite Rb_2AgBiI_6 absorber layer on the FTO/TiO_2 by spin coating at 6000 RPM for 30 s. The spin-coated perovskite layer was annealed on a hot plate at 70 ºC for 10 min to form the FTO/TiO_2/Rb_2AgBiI_6 interface. A hole transport material, copper thiocynate (CuSCN) spun at 2000 RPM on FTO/TiO_2/Rb_2AgBiI_6 for 20 s to form FTO/TiO_2/Rb_2AgBiI_6/CuSCN interface and annealed at 70 ºC for 10 min on the hot plate. For charge extraction, graphite was used as an electrode to form the FTO/TiO_2/Rb_2AgBiI_6/CuSCN/graphite interface. The same device architecture was also used as a photodetector to study switching behavior.

2.3 Material characterization

X-ray diffraction analysis was performed using an X-ray diffractometer (Bruker D8 Advance, Germany) with CuKα line (λ = 1.54056 Å) varying the 2θ values from 5° to 60° with an increment of 0.1°. The optical band gap of Rb_2AgBiI_6 film was estimated from the absorbance spectra recorded using a JASCO, V-670 UV-VIS-NIR spectrometer in the range of 200-650 nm. HITACHI, S-4800, Japan field emission scanning electron microscope (FE-SEM) with operating voltage 10 kV was used to observe the surface morphology of Rb_2AgBiI_6 film. The elemental compositional analysis of the Rb_2AgBiI_6 film was carried out using energy dispersive X-ray analysis (EDAX). Atomic force microscopy (NC-AFM) (JEOL, JSPM-5200) was used to investigate the surface topology in non-contact mode. Raman spectra were recorded using Raman spectroscopy (Renishaw InVia microscope Raman) in the range of 70-300 cm^{-1}. The spectrometer has backscattering geometry for the detection of Raman spectrum with the resolution of 1 cm^{-1}. The excitation source was a 532 nm line of He-Ne laser. The Raman laser's power and its spot size were kept > 5 mW and ~ 1 µm, respectively, to avoid possible heating effects on the sample. Thermogravimetric analysis (TGA) analysis was carried out by Mettler Toledo TGA/DSC/$STAR_e$ system. The Rb_2AgBiI_6 sample was heated in an air atmosphere at 1000 °C with a heating rate of 10 °C/min and airflow of 40 ml/min to study the thermal stability of Rb_2AgBiI_6. J-V characteristic of as-fabricated solar cell and switching behavior of photo detector were tasted using Potentiostat (Metrohm AUTOLAB PGSTAT302 N) 150 W and Xenon Lamp (PEC-L01) with illumination intensity of 100 mW/cm^2 (AM 1.5).

2.4 Theoretical Method

The electronic structure calculations were performed using density functional theory (DFT) within periodic boundary conditions as implemented in the Vienna Ab initio Simulation Package (VASP).[42-44] The PBE functional[45] was used for geometry optimizations and stability, while for electronic structures and optical calculations, the screened hybrid functional HSE06 with 25 % Hartree-Fock exchange was used.[46] The interactions between the valence electrons and the cores were described with the projected augmented wave (PAW) method.[47] A 3 × 3 × 3 Γ-centered Monkhorst-Pack[48] k-mesh and a 600 eV plane-wave cut off were used for all electronic structure calculations, while a tighter k-mesh of 5 × 5 × 5 was used for the optical calculations. The optical properties were calculated from the complex dielectric function, $\varepsilon(\omega) = \varepsilon_1(\omega) + i\,\varepsilon_2(\omega)$. The convergence criterion for the forces on each atom during optimization was set to 0.01 eV $Å^{-1}$.

3. Results and Discussion

X-ray diffraction patterns of the synthesized Rb_2AgBiI_6 film and powder are shown in Fig. 2(a). The presence of multiple peaks in the XRD pattern confirms the polycrystalline nature of the Rb_2AgBiI_6 film. The XRD spectra of synthesized samples match the simulated XRD pattern from DFT calculation, confirming the formation of the Rb_2AgBiI_6 phase. The diffraction planes at 2θ ~ 8.5º, 11.1º, 14º, 15º, 17º, 23.6º, 25.5º, 26.4º, 28.5º, 29.8º, 30º, 33º, 36.7º, 38 º, 43.2º, and 52.6º matches with simulation diffraction pattern. The inset in Fig. 2(a) shows the typical Raman spectra of as-synthesized Rb_2AgBiI_6 thin film in the range of 70-300 cm^{-1}. The three distinct peaks observed at 81 cm^{-1}, 113 cm^{-1}, and 140 cm^{-1} are

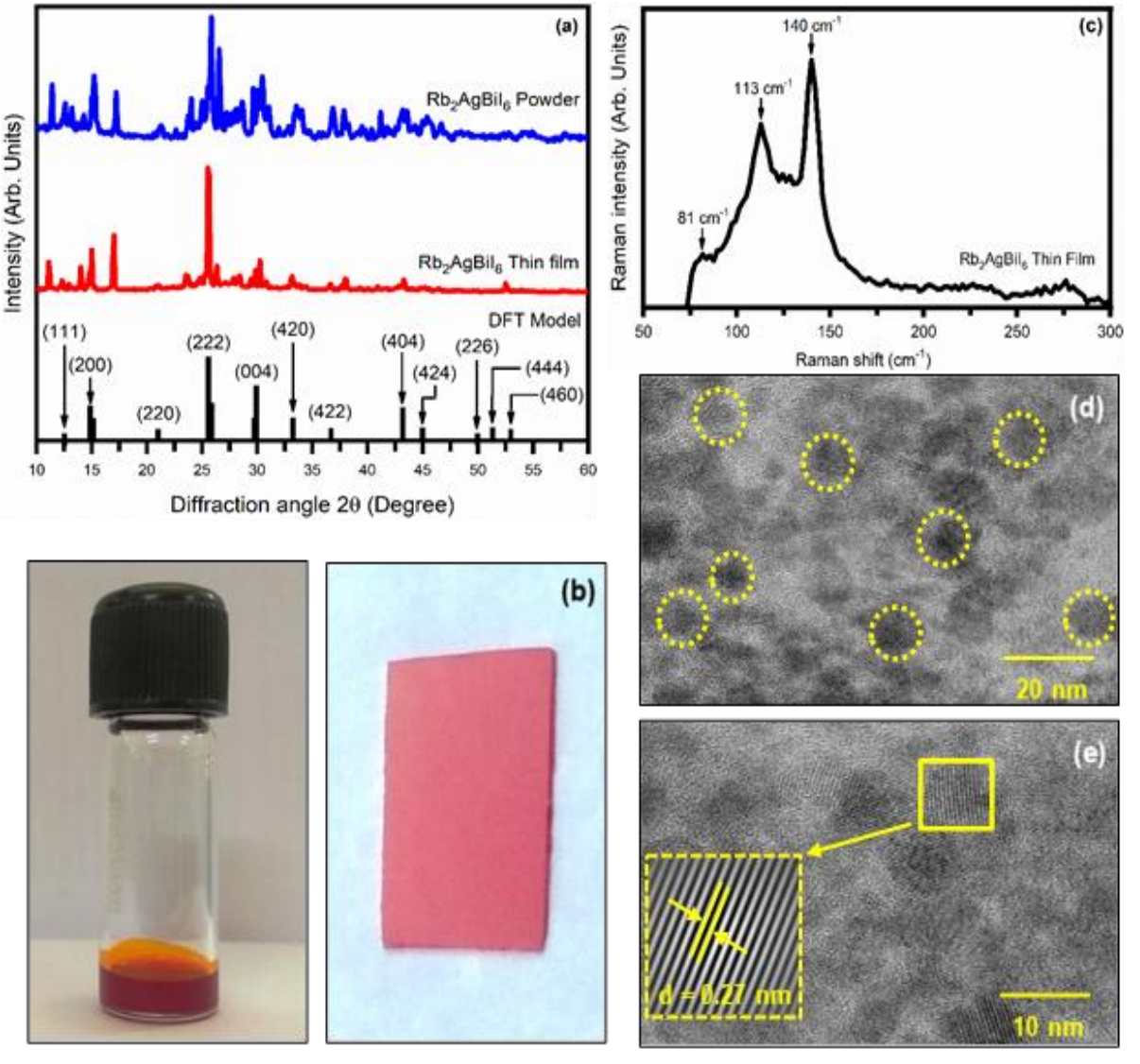

Fig. 2 (a) X-ray diffraction pattern (Cu Kα radiation) for the Rb_2AgBiI_6 nanocrystals and thin films indicating excellent crystallinity. The red reference pattern was simulated with VESTA Crystallographic Software using $Fm\bar{3}m$ space group and lattice parameters a = 12.07 Å for cubic Rb_2AgBiI_6. Raman spectroscopy of Rb_2AgBiI_6 nanocrystals at room temperature is shown as the inset. (b) Aactual photograph of Rb_2AgBiI_6 solution and thin film (c) Raman spectra of Rb_2AgBiI_6 film (d) TEM image of the Rb_2AgBiI_6 nanocrystals (e) HR-TEM image of one Rb_2AgBiI_6 nanoparticle with clear lattice resolution with an interplanar spacing of 0.27 nm can be resolved.

characteristics peaks of the Raman active modes of the synthesized Rb_2AgBiI_6 thin film. Both x-ray diffraction and Raman analyses reveal the formation of pure Rb_2AgBiI_6 phase without any impurity phase. Fig. 2(b) and (c) shows the TEM and High-resolution TEM (HR-TEM) images of Rb_2AgBiI_6, respectively. The parallel-arranged planes in the 10 nm size crystallites revealed interplanar spacing of 2.7 Å, which compares to 3.8 Å reported for Cs_2AgBiI_6 double perovskite by Creutzh *et al.*[49] TGA analysis reveals that the synthesized Rb_2AgBiI_6 double perovskite thin film is thermally stable up to 400 °C, with the weight remaining constant at ~ 34 mg [Fig. 3(a)]. Weight loss and, therefore, decomposition of the films only starts at temperatures above 400 °C, which decreases continuously up to 700 °C (weight loss ~ 17 mg). The UV-Visible absorption spectra [Fig. 3(b)] of Rb_2AgBiI_6 thin film reveals a strong absorption in the visible region starting from 600 nm to 200 nm (maximum absorption coefficient is ~ 8 × 10^3 cm^{-1}), which is suitable for the photovoltaic application. The band gap of the as-prepared Rb_2AgBiI_6 film was estimated from Tauc Plot[43] [inset in Fig. 3(b)] using the relation,

$$(\alpha h\nu)^{1/2} = B^{1/2}\left(h\nu - E_g\right) \quad (1)$$

where $h\nu$ is the photon energy, B is Tauc's constant, and α is the optical absorption coefficient.[50] Plotting $(\alpha h\nu)^{0.5}$ vs. photon energy (eV) [Inset in Fig. 3(b)], the optical band gap of $Rb_2AgBiI_6$is estimated to be ~ 1.98 eV. Consistent with the experimental estimation, a screened hybrid functional HSE06[51] DFT calculation predicts an indirect band gap of 1.96 eV [Fig. 4(b)]. The partial density of states (PDOS) plots

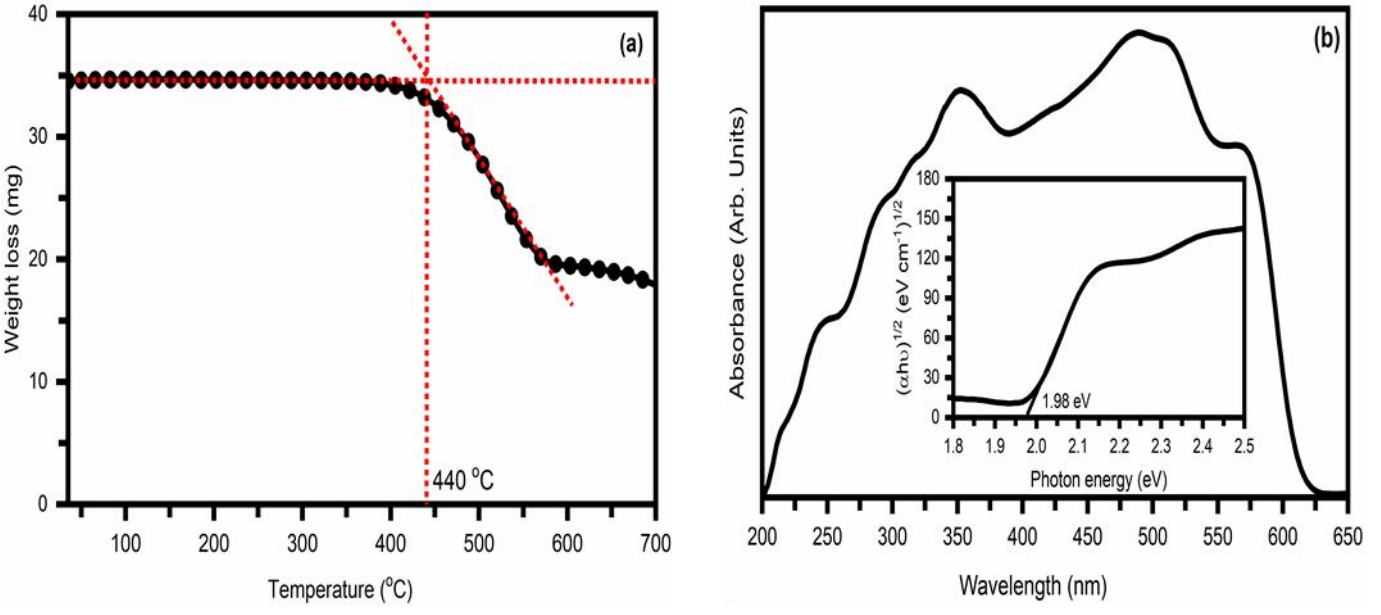

Fig. 3 (a) Thermogravimetric analysis (TGA) of Rb_2AgBiI_6 double perovskite. (b) UV-Visible absorbance of Rb_2AgBiI_6 double perovskite; the inset shows Tauc plot for Rb_2AgBiI_6 double perovskite.

[Fig. 4(c)] reveals I-p orbitals dominate valence bands, whereas the conductions are composed more of Bi-*p* orbitals. The predicted band gap of Rb_2AgBiI_6 is similar to the estimated band gap of synthesized Cs2AgBiI$_6$ double perovskite, with an estimated indirect band gap 1.75 eV.[35] A similar indirect band gap of 1.96 eV was reported for synthesized $(CH_3NH_3)_2AgBiI_6$ by Cheng *et al.*[39] Fig. 5(a), the real and imaginary part of the calculated dielectric functions

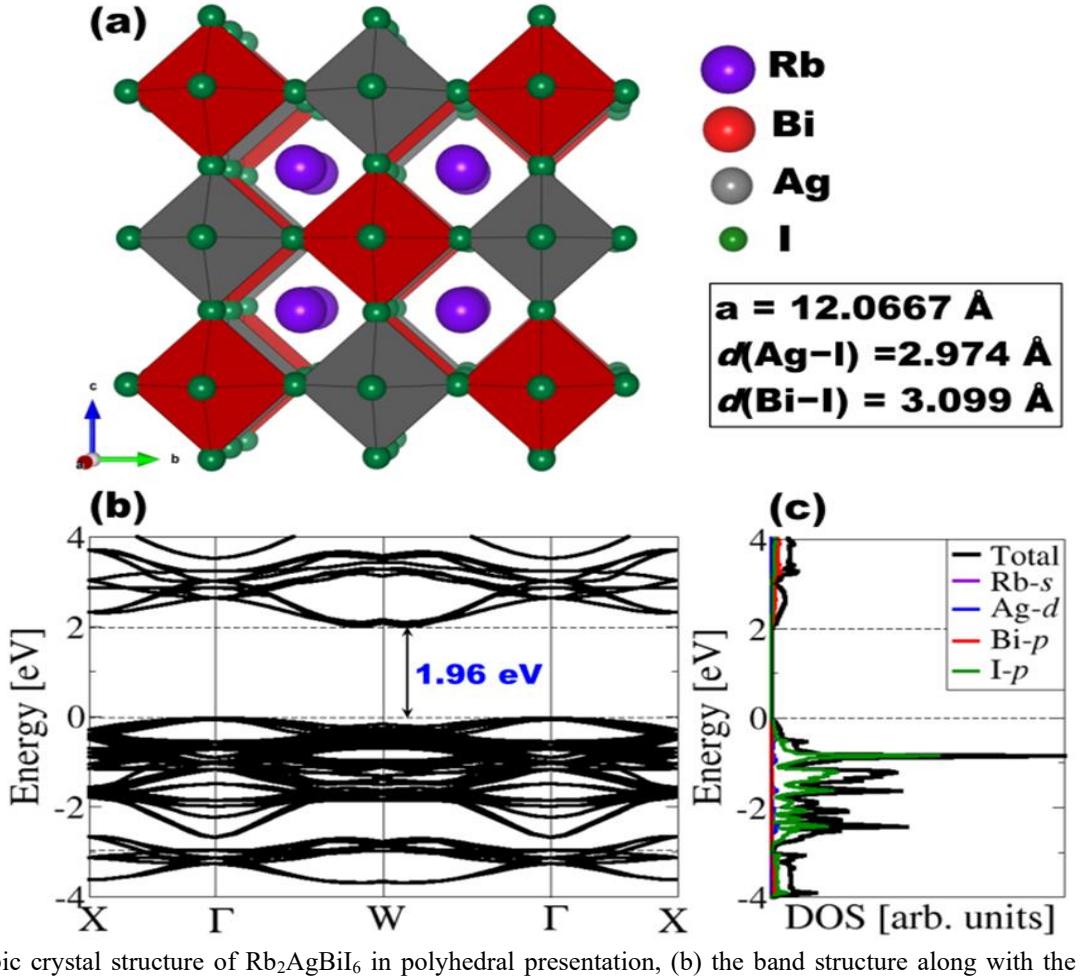

Fig. 4 (a) Cubic crystal structure of Rb_2AgBiI_6 in polyhedral presentation, (b) the band structure along with the high-symmetry directions of the Brillouin zone, and (c) the partial density of states (PDOS) of Rb_2AgBiI_6 predicted with HSE06 functional.

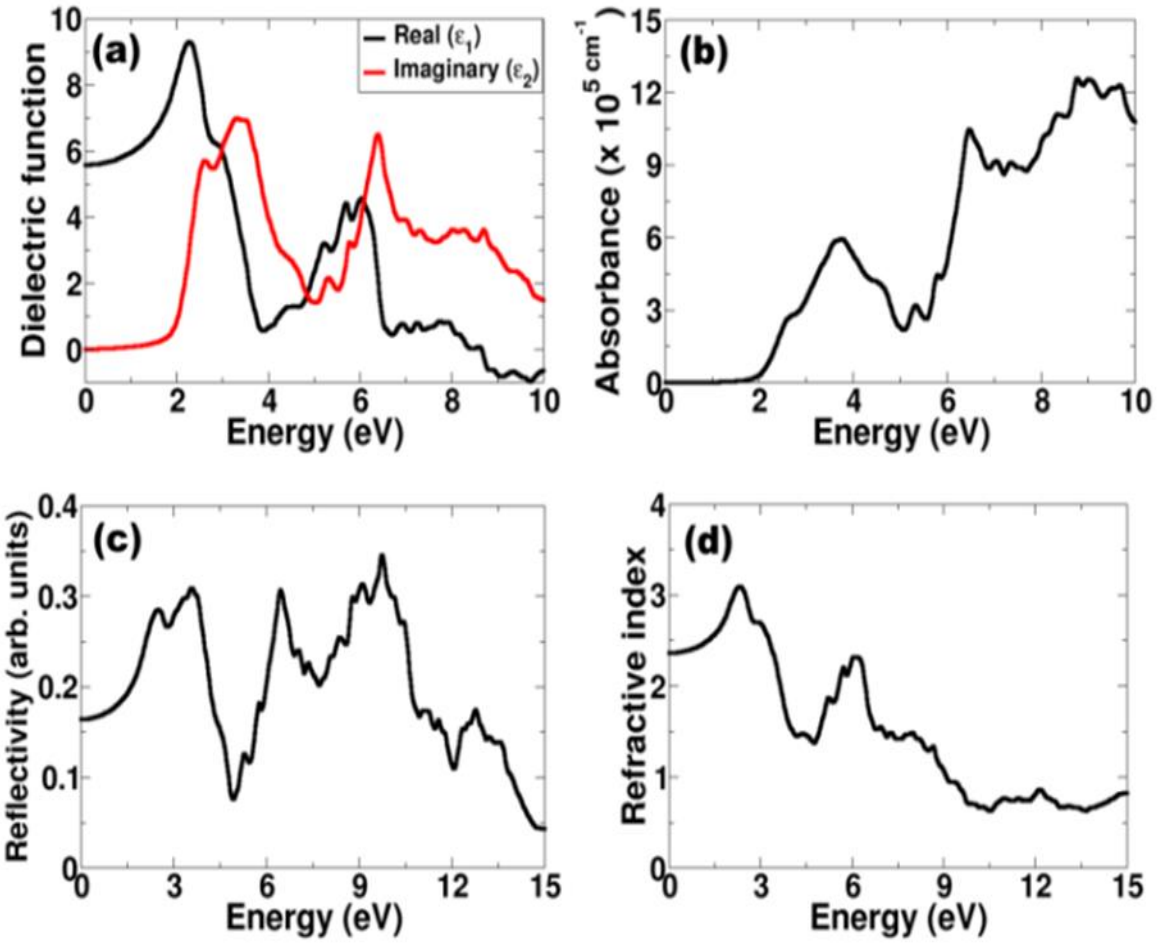

Fig. 5 Calculated (a) Dielectric function, (b) Absorbance, (c) Reflectivity, and (d) Refractive index of Rb_2ABiI_6 double perovskite.

for Rb_2AgBiI_6, predicts the dielectric constant at 5.52. The absorbance plot [Fig. 5(b)] shows that the absorption of Rb_2AgBiI_6 starts at around 2 eV, which corresponds to the fundamental band gap. The calculated optical reflectivity shown in Fig. 5(c) reveals that the reflectivity of Rb_2AgBiI_6 starts at ~ 16.31 % and has a maximum value of ~ 35.08 % at 9.75 eV. We have also plotted the refractive index in Fig. 5(d) and predicted the refractive index of Rb_2AgBiI_6 at 2.35. To assess the mechanical stability of the Rb_2AgBiI_6 film, we have calculated the elastic properties of Rb_2AgBiI_6 (Table 1). The elastic properties of $Cs_2AgBiCl_6$ and $Cs_2AgBiBr_6$ are also reported for comparison. The calculated C11, C12, and C44 elastic constants of Rb_2AgBiI_6 are predicted at 35.09, 19.81, and 715 GPA, whiles the bulk (B), shear (G), Young's (E) moduli, and poison ratio (ν) are calculated at 29.90, 7.34, 20.06, and 0.36. All the calculated single-crystal elastic constants satisfy Born-Huang's mechanical stability criteria for cubic structures,[52] thereby confirming the mechanical stability of Rb_2AgBiI_6 under ambient conditions. Similar elastic properties were predicted for $Cs_2AgBiCl_6$ and $Cs_2AgBiBr_6$ by Ghebouli *et al.,*[53] as shown in Table 1. The smaller shear modulus than the bulk and Young's moduli suggests that Rb_2AgBiI_6 will be more prone to shear deformation than compressive deformation.

Table 1. Calculated elastic stiffness constants (Cij), bulk modulus (B), shear modulus (G), Young's modulus (E), and Possion's ratio (ν) of Rb2AgBiI6 at 0 GPa.

Parameter	Rb_2AgBiI_6	$Cs_2AgBiCl_6$ [53]	$Cs_2AgBiBr_6$ [53]
C11	35.09	39.38	24.55
C12	19.81	13.76	13.56
C44	07.15	08.71	07.52
B	24.90	22.30	17.22
G	07.34	10.16	06.63
E	20.06	26.48	17.64
ν	00.36	00.30	00.33

Field emission scanning electron microscopy (FE-SEM) was used to study the surface morphology of as-prepared Rb_2AgBiI_6 thin film. The FESEM micrographs of the Rb_2AgBiI_6 film at x 500 resolution shown in Fig. 6 (a) reveal a dense and uniform Rb_2AgBiI_6 film in the overall surface area. The elemental composition of the as-deposited Rb_2AgBiI_6 film was investigated using EDAX, and Fig. 6(b)-(f) shows the elemental mapping analysis of Rb, Ag, Bi, and I concentration. The double perovskite Rb_2AgBiI_6 film is rich in Rb and I, with similar atomic percentages of Ag and Bi. The surface topology properties have been studied using atomic

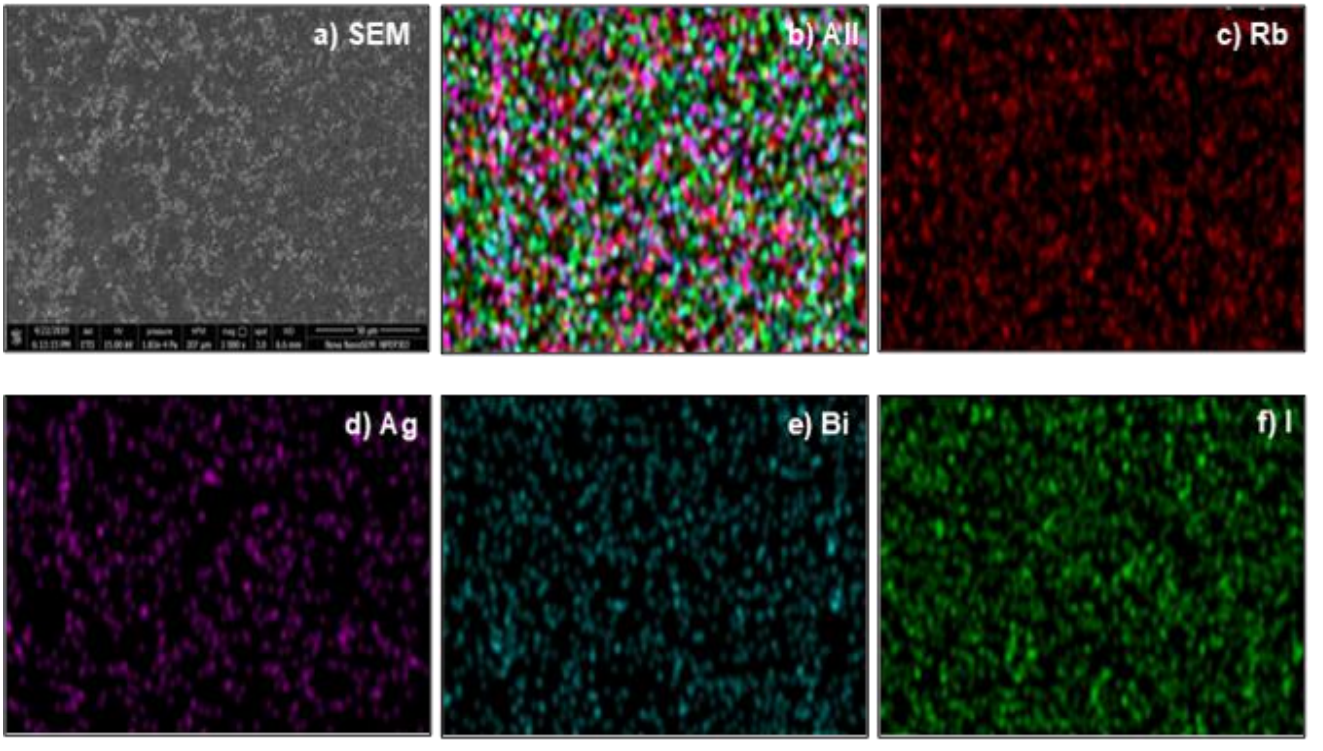

Fig. 6 (a) FE-SEM micrograph of Rb_2AgBiI_6 thin film. (b) Elemental mapping for thin film. (c) Rb contains in Rb_2AgBiI_6 thin film. (d) Ag contains Rb_2AgBiI_6 thin film. (e) Bi contain in Rb_2AgBiI_6 thin film. (f) I contain a Rb_2AgBiI_6 thin film. The elemental mapping suggests an even distribution of chemical constituents in the Rb_2AgBiI_6 thin film.

force microscopy (AFM). The 2D AFM micrograph of Rb_2AgBiI_6 thin film [Fig. 7(a)] indicates that the thin film surface is smooth, and the vertical height between the highest and lowest features is less than 50 nm. The root mean square (RMS) roughness and average surface roughness achieved using a 3D image [Fig. 7(b)] was found to be 46 nm. The images show a continuous and dense film without defects such as cracks, pinholes, and protrusion.

The fabricated planer heterojunction Rb_2AgBiI_6 based perovskite solar cell device structure schematic [FTO/TiO_2/Rb_2AgBiI_6/CuSCN/graphite] is shown in Fig. 8(a). The TiO_2 layer act as electron transport material and CuSCN act as hole transport material. The fabricated double perovskite Rb_2AgBiI_6 based solar cell was tested for 0 V to 5 V bias voltage. The maximum photocurrent is of Isc ~ 80 μA, and the active area of the device is 0.15 cm^2 with a current

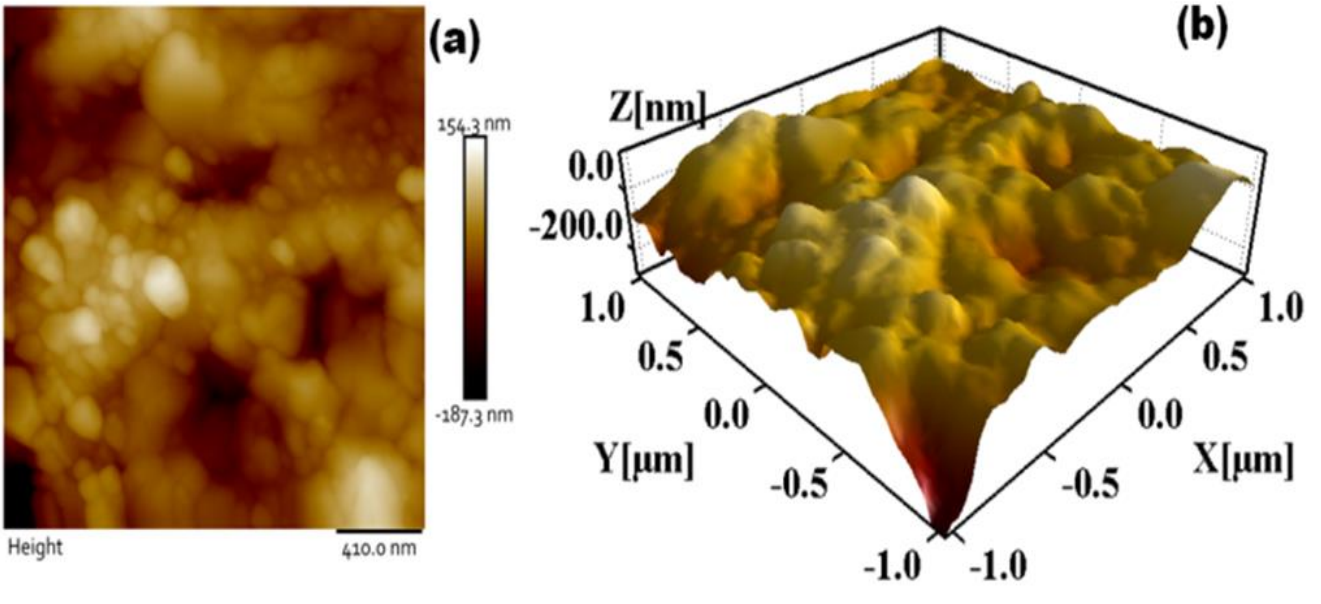

Fig. 7 (a) Two-dimensional (2D) AFM images of Rb_2AgBiI_6 thin film (b) Three-dimensional (3D) AFM images of Rb_2AgBiI_6 thin film prepared at optimized process parameters.

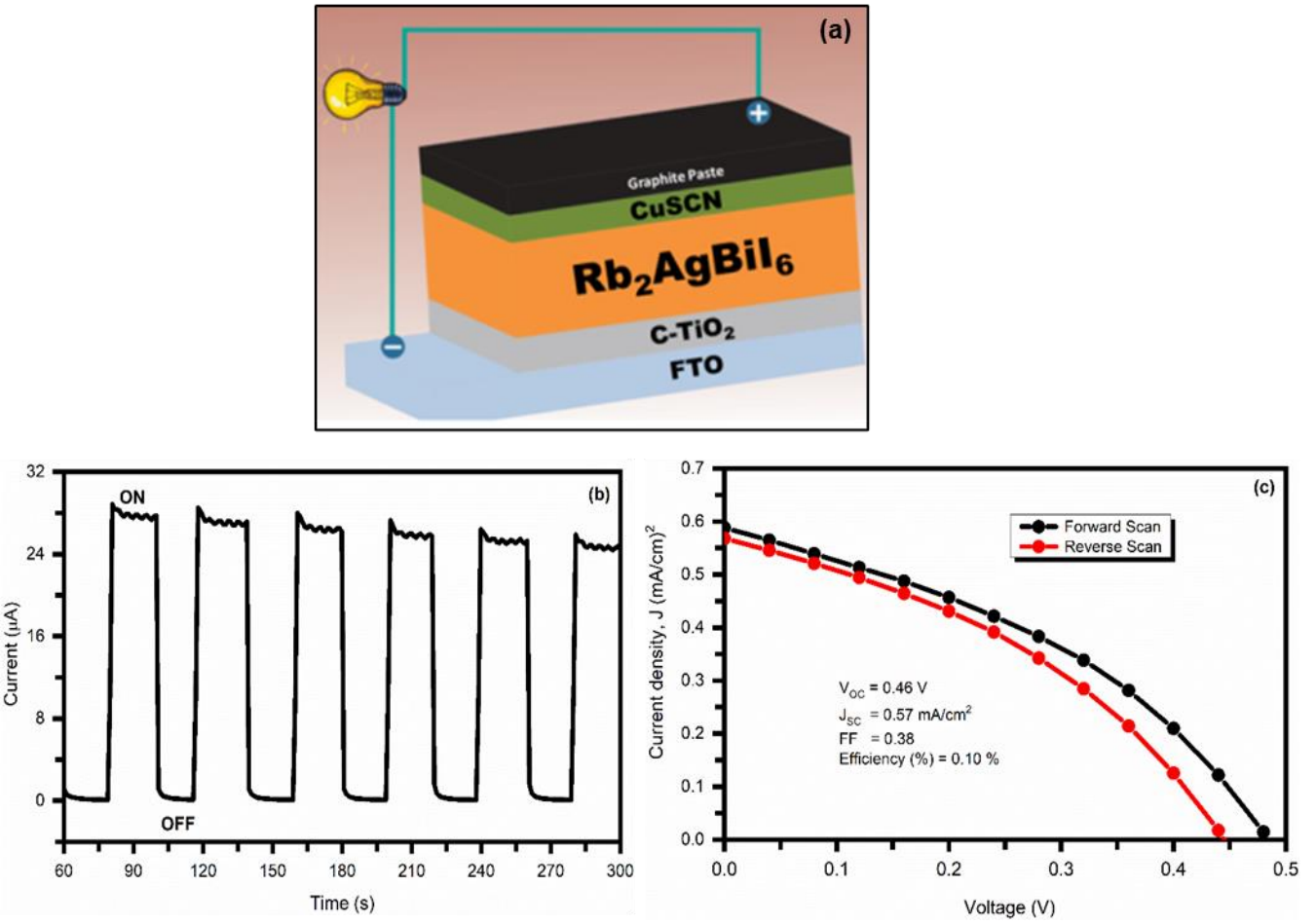

Fig. 8 (a) Schematic photovoltaic device fabricated with Rb_2AgBiI_6 thin films in the glass/C-TiO_2/Rb_2AgBiI_6/CuSCN/Graphite architecture. (b) Rb_2AgBiI_6 based photo-detector to study the switching behavior and (c) Current-voltage characteristics of the fabricated Rb_2AgBiI_6 PV device, measured under light illumination with 100 mW/cm^2 intensity.

density Jsc ~ 0.57 mA/cm^2. The device's open-circuit voltage is ~ 0.46 V, with a fill factor FF of ~ 38 % [Fig. 8 (c)]. The measured power conversion efficiency of the Rb_2AgBiI_6 PSC is ~0.10%, which is relatively low due to the high series resistance. While the devices' efficiency is low, the Rb_2AgBiI_6 absorber layer was not processed after deposition with any high-temperature or chemical means. We expect that with further optimization of the synthesis conditions and device architecture, the PV efficiency should increase.

We have also attempted to make Rb_2AgBiI_6 based photo detector using the same PSC device structure to study the switching behavior of synthesized double Rb_2AgBiI_6 perovskite. The photoresponse for the Rb2AgBiI6 double perovskite photo detector was analyzed under dark and light conditions simultaneously using a solar simulator and AUTOLAB potentiostat without a bias voltage. Fig. 8(b) shows the typical switching behavior of the Rb_2AgBiI_6 photo detector for 5 min. The decrease in the photocurrent may be due to the thermodynamic instability of Ag.[54] For better performance, further optimization is needed, mainly in the film thickness.

4. Conclusions

In summary, by employing synergetic experimental and computational first-principles DFT calculations, we report the synthesis of lead-free halide double perovskite Rb_2AgBiI_6, providing insights into the structural, thermal and mechanical stability, electronic and optical properties. We have developed a single-step solution process synthetic route for producing the double perovskite Rb_2AgBiI_6 films via a fast and efficient spin-coating method. The resulting Rb_2AgBiI_6 film is demonstrated to crystallize in a double perovskite cubic $Fm\bar{3}m$ space group and possesses an indirect band gap of ~ 1.98 eV, estimated from UV-Visible spectroscopy analysis and validated by hybrid DFT calculations. TGA analyses reveal that the as-synthesized Rb_2AgBiI_6 double perovskite has maximum thermal stability up to ~ 440ºC. Fabricated Rb_2AgBiI_6 based photo-detector and PSC with device architecture FTO/TiO_2/Rb_2AgBiI_6/CuSCN/graphite is demonstrated to have Voc of ~ 0.46 V, Isc ~ 0.57 mA cm^{-2}, FF ~ 0.38, with the PCE estimated to be 0.10 %. With the further optimization of synthesis condition and device fabrication, there an enormous opportunity to increase the device efficiency towards the development of highly efficient halide double Rb_2AgBiX_6 (X = Cl, Br, and I) perovskites for diverse environmentally friendly optoelectronic applications.

Acknowledgement
Ajinkya Bhorde is thankful to the Department of Science and Technology (DST), Government of India, for the INSPIRE fellowship. Ravindra Waykar and Shruthi Nair are thankful to the Ministry of New and Renewable Energy (MNRE), Government of India, for the financial support under the National Renewable Energy Fellowship (NREF) program. Ganesh Lonkar is thankful to University Grant Commission for Dr. D. S. Kothari postdoctoral fellowship. All authors are thankful to Central Instrumentation Facility (CIF), Savitribai Phule Pune University, for providing analytical facilities. One of the authors, Sandesh Jadkar, is thankful to the University Grants Commission (UPE program), New Delhi and Indo-French Centre for the Promotion of Advanced Research-CEFIPRA, Department of Science and Technology, New Delhi for special financial support. Nelson Y. Dzade and Sachin Rondiya acknowledge the UK Engineering and Physical Sciences Research Council (EPSRC) for funding (Grant No. EP/S001395/1). This work has also used the Advanced Research Computing computational facilities at Cardiff (ARCCA) Division, Cardiff University, and HPC Wales.

Conflict of Interest
There is no conflict of interest.

Supporting Information
Not applicable

References
[1] S. Creutz, E. Crites, M. De Siena, and D. R. Gamelin, *Nano Lett*., 2018, **18**, 1118-113, doi: 10.1021/acs.nanolett.7b04659.
[2] P. Cheng, T. Wu, Y. Li, L. Jiang, W. Deng, and Keli Han, *New J. Chem.*, 2017, **41**, 9598-9601, doi: 10.1039/C7NJ02365K.
[3] G. Hodes, *Science,* 2013, **342**, 317-318, doi: 10.1126/science.1245473.
[4] M. A. Green, A. H. Baillie, and H. J. Snaith, *Nat. Photonics,* 2014, **8**, 506-514, doi: 10.1038/nphoton.2014.134.
[5] D. T. Moore, H. Sai, K. W. Tan, D. M. Smilgies, W. Zhang, H. J. Snaith, U.Wiesner, and L. A. Estroff, *J. Am. Chem. Soc.,* 2015, **137**, 2350-2358, doi: 10.1021/ja512117e.
[6] U. Koster, *Phys. Status Solidi B*., 1978, **48**, 313-321, doi: 10.1002/pssa.2210480207.
[7] C. Li, X. Lu, W. Ding, L Feng, Y. Gao, Z. Guo, *Acta Crystallogr*. S, 2008, **64**, 702–707, doi: 10.1107/S0108768108032734.
[8] Q. Dong, Y. Fang, Y. Shao, P. Mulligan, J. Qiu, L. Cao, J. Huang, *Science*, 2015, **347**, 967–970, doi: 10.1126/science.aaa5760.
[9] V. D'Innocenzo, G. Grancini, M. J. Alcocer, A. R. Kandada, S. D. Stranks, M. Lee, G. Lanzani, H. Snaith, A. Petrozza, *Nat. Commun*., 2014, **5**, 3586-3591, doi: 10.1038/ncomms4586.
[10] M. Hirasawa, T. Ishihara, T. Goto, K. Uchida, N. Miura, *Physica B*, 1994, **201**, 427–430, doi: 10.1016/0921-4526(94)91130-4.
[11] J. Burschka, N. Pellet, S. J. Moon, H. Humphry-Baker, P. Gao, M. K. Nazeeruddin, M. Grätzel, *Nature,* 2013, **499**, 316-319, doi: 10.1038/nature12340.
[12] M. Liu, M. B. Johnston, H. J. Snaith, *Nature,* 2013, **501**, 395, doi: 10.1038/nature12509.
[13] Z. Haiming, F. Yongping, M. Fei, W. Xiaoxi, G. Zizhou, D. Qi, G. M. Martin, T. Tuan, J. Song, *Nat. Mater*., 2015, **14**, 636-642, doi: 10.1038/nmat4271.
[14] Z. Tan, R. S. Moghaddam, M. L. Lai, P. Docampo, R. Higler, F. Deschler, M. Price, A. Sadhanala, L. M. Pazos, D. Credgington, F. Hanusch, T. Bein, H. J. Snaith, R. H. Friend, *Nat. Nanotechnol,* 2014, **9**, 687-692, doi: 10.1038/nmat4271.
[15] X. Jun, Y. Fei, Z. Yawen, C. Shi, Y. Huakang, Z. Qing, Z. Rongguang, V. Hilmi, S. Xiaowei, H. Alfred, X. Qihua, *ACS Nano*., 2016, **10**, 6623-6630, doi: 10.1021/acsnano.6b01540.
[16] Gurudayal, S. Dharani, H. Mulmudi, H. Lydia, B. James, G. Michael, M. Nripan, *Nano Lett*., 2015, **15**, 3833-3839, doi: 10.1021/acs.nanolett.5b00616.
[17] J. Luo, Jeon-Hyeok T. M. Matthew, S. Marcel, K.N. Mohammad, P. Nam-Gyu, T. David, J. Hong F. Jin, G. Michael, *Science*, 2014, **345**, 1593-1596, doi: 10.1126/science.1258307.
[18] A. Kojima, K. Teshima, Y. Shirai, T. Miyasaka, *J. Am. Chem. Soc*., 2009, **131**, 6050–6051, doi: org/10.1021/ja809598r.
[19] J. H. Heo, S.H. Im, J.H. Noh, T. N. Mandal, C. S. Lim, J. A. Chang, Y. H. Lee, H. Kim, A. Sarkar, M. K. Nazeeruddin, *Nat. Photonics,* 2013,**7**, 486–491, doi: 10.1038/nphoton.2013.80
[20] NREL, Perovskite Efficiency Chart, https://www.nrel.gov/pv/assets/pdfs/best-research-cell-efficiencies.20190923.pdf, accessed 23 September 2019.
[21] C. Min, J. Ming-Gang, F. Hector, D.C. Alexander, K. O Luis, H. Zafer Z. Yi, S. Tianyi, Q. Yabing, *Nat. Comm.*, 2019, **10**, doi: 10.1038/s41467-018-07951-y.
[22] A. Babayigit, A. Ethirajan, M. Muller, *Nat. Mater*., 2016, 15, 247-252, doi: 10.1038/nmat4572.
[23] M. Lei, J. You, Y. Yang, *Nat. Comm.*, 2018, **9**, 5265, doi: 10.1038/s41467-018-07255-1.
[24] N. Guangda, G. Xudong, W. Liduo, *J. Mater. Chem. A,* 2015, **3**, 8970-8980, doi: 10.1039/C4TA04994B.
[25] N. Wang, Z. Yuanyuan, J. Ming-Gang, F. G. Hector, D. Tao, P. Shuping, C. Xiao, N. Zeng, P. Padture, W. Xiao, *Adv. Energy Mater*., 2016, **6**, 1601130-1601140, doi: 10.1002/aenm.201601130.
[26] K. Z. Du, W. Meng, X. Wang, Y. Yan, D. B. Mitzi, *Angew. Chem. Int. Ed.*, 2017, **56**, 8158–8162, doi: 10.1002/aenm.201601130.
[27] Z. Zhang, L. Xiaowei, X. Xiaohong, W. Zhuo, H. Zhongbing, L. Binglong, G. Yun, *J. Phys. Chem. Lett*., 2017, **8**, 4300–4307, doi: 10.1021/acs.jpclett.7b01952.
[28] M. Chen, J. Ming-Gang, D. C. Alexander, Z. Yingxia, L.G. Ronald, G. Jiajun, C. Xiao, Z. Yuanyuan, P. P. Nitin, *Joule,* 2018, **2**, 558–570, doi: 10.1016/j.joule.2018.01.009.
[29] C. Zuo, L. Ding, *Angew. Chem. Int. Ed.,* 2017, **56**, 6528–6532, doi: 10.1002/anie.201702265.

[30] S. Shao, L. Jian, P. Giuseppe, F. Hong-Hua, R. B. Graeme, H. Gert, L. Brink, A. Jan, A. Maria, *Adv. Energy Mater.*, 2018, **8**, 1702019, doi: 10.1002/aenm.201702019.
[31] Z. Zhang, X. Li, X. Xia, Z. Wang, Z. Huang, B. Lei, Y. Gao, *J. Phys. Chem. Lett.*, 2017, **8**, 4300–4307, doi: 10.1021/acs.jpclett.7b01952.
[32] M. B. Johansson, H. M. Zhu, E. M. Johansson, *J. Phys. Chem. Lett.,* 2016, **7**, 3467– 3471, doi: 10.1021/acs.jpclett.6b01452.
[33] B. Fan, H. Yonghong, H. Yanqiang, Q. Ting, M. Xiaoliang, Z. Shufang, *Sol. Energ. Mat. Sol. C.*, 2018, **184**, 15–21, doi: 10.1016/j.solmat.2018.04.032.
[34] T. M. Eric, R. B. Molly, W. Wolfgang, M.W. Patrick, *Chem. Mater.*, 2016, **28**, 1348-1354, doi: 10.1021/acs.chemmater.5b04231.
[35] A. H. Slavney, T. Hu, A. M. Lindenberg, H. I. Karunadasa, *J. Am. Chem. Soc*., 2016, **138**, 2138-2141, doi: 10.1021/jacs.5b13294.
[36] E.T. McClure, M. R. Ball, W. Windl, P. M. Woodward, *Chem. Mater*., 2016, **28**, 1348-1354, doi: 10.1021/acs.chemmater.5b04231.
[37] G. Volonakis, M. R. Filip, A. A. Haghighirad, N. Sakai, B. Wenger, H. J. Snaith, F. Giustino, *J. Phys. Chem. Lett*., 2016, **7**, 1254-1259, doi: 10.1021/acs.chemmater.5b04231.
[38] S. Michael, M. Taisuke, D. Konrad, S. Ji-Youn, U. Amita, M. Z. Shaik, C. Juan-Pablo, R. T. Wolfgang, A. Antonio, H. Anders, G. Michael, *Science,* 2016, **324**, 206-209, doi: 10.1126/science.aah5557.
[39] C. Pengfei, W. Tao, L. Yajuan, J. Lei, D. Weiqiao, H. Keli, *New J.Chem.*, 2017, **41**, 9598-9601, doi: 10.1039/C7NJ02365K.
[40] I. Femi, W. Rui, W. Zhao-Kui, M. Xing-Juan, W. Qiang, W.; Kai-Li, Z. Yue, L. Liang-Sheng, Y. Yang, *Nano Lett.*, 2019, **19**, 2066−2073, doi: 10.1021/acs.nanolett.9b00238.
[41] C. Yichuan, Z. Linrui, Z. Yongzhe, G. Hongli, Y. Hui, *RSC Adv*., 2018, **8**, 10489–10508, doi: 10.1039/C8RA00384J.
[42] G. Kresse, J. Hafner, *Phys. Rev. B*,1993, **47**, 558−561, doi: 10.1103/PhysRevB.47.558.
[43] G. Kresse, J. Hafner, *Phys. Rev. B*, 1994, 49, 14251−14269, doi: 10.1103/PhysRevB.49.14251.
[44] G. Kresse, J. Furthmüller, *Phys. Rev. B*, 1996, **54**, 11169−11186, doi: 10.1103/PhysRevB.54.11169.
[45] J. Perdew, K. Burke, M. Ernzerhof, *Phys. Rev. Lett.*, 1996, **77**, 3865−3868, doi: 10.1103/PhysRevLett.77.3865.
[46] A.V. Krukau, O. A. Vydrov, A. F. Izmaylov, G. E. Scuseria, *J. Chem. Phys.*, 2006, **125**, 224106, doi: org/10.1063/1.2404663
[47] P. Blochl, *Phys. Rev. B*, 1994, **50**, 17953−17979, doi: 10.1103/PhysRevB.50.17953.
[48] H. J. Monkhorst, J. D. Pack, *Phys. Rev. B.*, 1976, **13** 5188−5192, doi: 10.1103/PhysRevB.13.5188.
[49] S. E. Creutz, E. N. Crites, M. C. De Siena, D. R. Gamelin,. *Nano Lett.,* 2018, **18**, 1118-1123, doi: 10.1021/acs.nanolett.7b04659.
[50] J. Tauc, *Mater. Res. Bull*., 1968, **3**, 37-46, doi: 10.1016/0025-5408(68)90023-8.
[51] A.V. Krukau, O. A. Vydrov, A. F. Izmaylov, G. E. Scuseria, *J. Chem. Phys.*, 2006, **125**, 224106, doi: 10.1063/1.2404663.
[52] J. Wang, S.Yip, *Phys. Rev. Lett.*, 1993, **71**, 4182-4185, doi: 10.1103/PhysRevLett.71.4182.
[53] M. A. Ghebouli, T. C. B. Ghebouli, M. Fatmi, *Chinese J. Phys.*, 2018, **56**, 323-330, doi: 10.1515/msp-2017-0017.
[54] N. S. Christopher, W. Aron, O. S. David, *ACS Energy Lett*., 2016, **1**, 949−955, doi: 10.1021/acsenergylett.6b00471.